Synthesis and Characterization of Copper Nanoferrite and Magnesium-Nickel-Silver Doped Copper Nanoferrites

PRIYANKA NAIK[1,2,] and SHIVRAJ G. GOUNHALLI[1,2,*,]

[1]Department of Physics, Smt. Veeramma Gangasiri College for Women, Kalaburagi-585102, India
[2]Department of Physics, Karnataka State Akkamahadevi Womens University, Vijayapur-586108, India

*Corresponding author: E-mail: sgg19777@gmail.com

The sol-gel approach was used to synthesize the copper nanoferrite and magnesium-nickel-silver doped copper nanoferrites in the present work. Several methods were used to characterize the synthesized nanoferrites, including X-ray diffraction (XRD), Fourier-transform infrared spectroscopy (FTIR), field emission scanning electron microscopy (FESEM) and UV-visible spectroscopy. FTIR spectroscopy revealed metal ion peaks at 547-569 cm^{-1}. XRD evaluation indicated that the typical crystallite size was between 20 and 26 nm and the FESEM exhibited non-uniform forms in the synthesized nanoferrites. Elemental analysis revealed the presence of copper, magnesium, nickel and silver in the doped nanoferrites. UV-visible spectroscopy revealed that the direct optical band gap of 1.61 eV for pure copper nanoferrite, 1.53 eV for $Cu_{0.5}$ and 1.36 eV for $Cu_{0.7}$. The hysteresis loop of $CuFe_2O_4$ nanoparticles was studied to examine their magnetic properties. These findings implies that the synthesized nanoferrites have potential uses in semiconducting device applications and magnetic data storage.

Keywords: Sol-gel method, Nanoferrites, Magnetic properties.

INTRODUCTION

Ferrites are the ceramic materials that exhibit magnetic properties and are composed of iron oxide (Fe_2O_3) and one or more other metallic oxides. Copper ferrites differ from others due to their distinct molecular properties and various applications. Copper ferrites are noteworthy materials, such as $CuFe_2O_4$, are composed of Cu^{2+} and Fe^{3+} ions arranged in a crystal lattice structure. Copper ions (Cu^{2+}) occupy tetrahedral sites, while iron ions (Fe^{3+}) occupy octahedral sites. This arrangement results in a spinel structure, with copper ions in a tetrahedral configuration and iron ions in an octahedral arrangement [1]. Copper nanoferrites are used in various applications, including catalysis, electronics and medicine. However, one drawback of copper ferrites is their low saturation magnetization, which restricts their use in various applications. To solve this restriction, researchers looked into doping copper ferrites with nickel, magnesium and silver [2].

When tetrahedral and octahedral molecules are introduced into copper ferrites' crystal lattice structure, their locations shift. This leads to increased saturation magnetization and better magnetic characteristics. Copper nanoferrite and magnesium-nickel-silver doped copper nanoferrites can be synthesized using a different chemical processes. Co-precipitation, hydrothermal synthesis and the sol-gel techniques are among the most often utilized processes. The sol-gel process, in particular, has sparked interest because to its ability to manufacture high-quality, homogenous nanoparticles with precise size and shape [3-6]. In this work, copper nanoferrite and magnesium-nickel-silver doped copper nanoferrites were synthesized and characterized using the sol-gel method.

This study analyzed the fundamental and stage characteristics of electrochemically deposited copper-bismuth, copper-magnesium and cupronickel films. Copper, bismuth, nickel, and magnesium had been selected for the component composition due to their ability to form single-stage structures, which can significantly affect the erosion characteristics of films under extreme conditions [7,8]. When the erosion resistance of thin films was investigated, it was found that a reduction in the concentration of copper-containing phases enhanced their

resistance to oxidation and degradation [9]. The conditions of the combination are known to influence the stage arrangement, strength and consumption attributes of the created films. From the perspective of fundamental research and practical uses, NiFe films with a structured orientation are of significant interest [10].

Overall, the research into copper nanoferrites and their doped equivalents has led to new possibilities for magnetic materials with enhanced properties and applications. The positions of tetrahedral and octahedral molecules in the crystal lattice structure were changed and the applications of these mixtures were evaluated. Recognizing the chemical characteristics and synthesis techniques of these materials enables researchers to continuously create and improve magnetic materials for diverse technological advancements [10,11].

EXPERIMENTAL

Copper nitrate [$Cu(NO_3)_2 \cdot 6H_2O$], ferric nitrate [$Fe(NO_3)_3 \cdot 9H_2O$], citric acid [$C_6H_8O_7 \cdot H_2O$], nickel(II) nitrate hexahydrate [$Ni(NO_3)_2 \cdot 6H_2O$], silver nitrate hexahydrate [$AgNO_3 \cdot 6H_2O$], ammonia solution and magnesium nitrate hexahydrate [$Mg(NO_3)_2 \cdot 6H_2O$] were procured from Sigma-Aldrich, USA.

Synthesis: The metal nitrates and citric acid were mixed in distilled water and stirred thoroughly. The solution was then heated to 90 °C to facilitate the evaporation of water. Then, NH_3 was added dropwise to the mixture to increase the pH level. As evaporation occurs, the solution becomes viscous and forms a gel. The heating process continues to convert the gel into ash. Finally, the resulting powder was ground using a mortar and pestle and then calcined at 300 °C for 2 h [12,13].

RESULTS AND DISCUSSION

XRD (X-ray diffraction) analysis: Fig. 1 shows the XRD spectra analyzed for the phase purity of the samples $CuFe_2O_4$ termed as Cu, $Mg_{0.13}Ni_{0.13}Ag_{0.04}Cu_{0.7}Fe_2O_3$ termed as $Cu_{0.7}$ and $Mg_{0.21}Ni_{0.21}Ag_{0.08}Cu_{0.5}Fe_2O_3$ termed as $Cu_{0.5}$. The peaks corresponding to the planes of spinel ferrite are (220), (311), (400), (511) and (440), which align well with JCPDS card no. 74-2081. The strong peak at (311) is significantly more intense and the sharp, narrow peaks suggest the crystalline nature and purity of the samples. The sample exhibits a cubic spinel structure with an *Fd3m* spatial group. The size of the crystallites was determined using Debye-Scherrer's formula [13-15]:

$$D = \frac{k\lambda}{\beta\cos\theta} \tag{1}$$

where D represents the size of crystallite; β denotes the line broadening measured at the full width at half maximum (FWHM) of the most intense peak; k is the Scherrer's constant; θ is the Bragg's angle and λ is the wavelength of the X-ray [16]. The crystallite sizes were determined to range from 14 to 24 nm.

FT-IR spectral studies: Fig. 2 shows the FT-IR spectra of the functional groups in synthesized copper ferrite and Mg-Ni-Ag doped copper ferrites. These were analyzed using FTIR spectroscopy in the range of 4000-500 cm^{-1}. This technique utilizes infrared radiation to study atomic or molecular vibrations and their intensities, serving as an effective method for
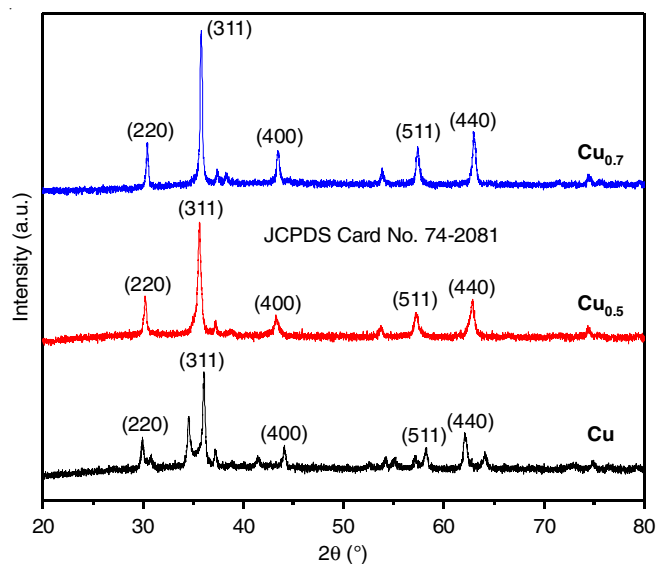
Fig. 1. X-ray diffraction analysis for synthesized nanoparticles Cu, $Cu_{0.5}$, $Cu_{0.7}$
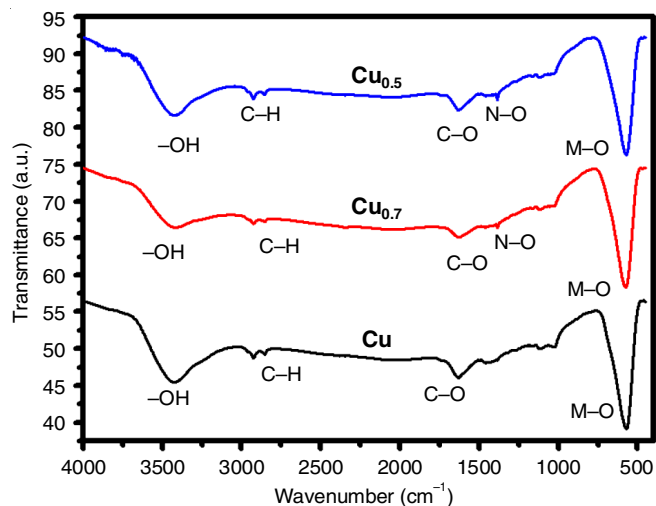
Fig. 2. FTIR analysis for synthesized nanoparticles Cu, $Cu_{0.5}$, $Cu_{0.7}$

identifying local chemical bonds [16,17]. This study investigates the structural features of spinel ferrite by analyzing the FTIR spectra of both pure copper ferrite and Mg-Ni-Ag doped copper ferrites. All the spinel ferrites display broad metal-oxygen bands in their FTIR spectra, typically observed in the range of 600-500 cm^{-1}. A prominent peak in the range of 3700-3200 cm^{-1} is attributed to the stretching vibrations of O-H bonds. Moreover, bands at 1617 cm^{-1} are linked to the C-O stretching mode, which results from the adsorption of ambient CO_2 onto the nanoparticle surfaces. The peak at 1370 cm^{-1} is due to the bending vibrations of N-O bonds. Finally, the transmission band at 585 cm^{-1} is associated with the stretching vibrations of metal ions [18-20].

SEM studies: The SEM images of the synthesized ferrites are shown in Fig. 3a-c for various molar fractions. All images clearly depict the grains and their corresponding grain boundaries. The spectra reveal aggregated grain boundaries between the grains, featuring an irregular distribution of particles [19]. The average grain sizes of the nanoferrites were analyzed using
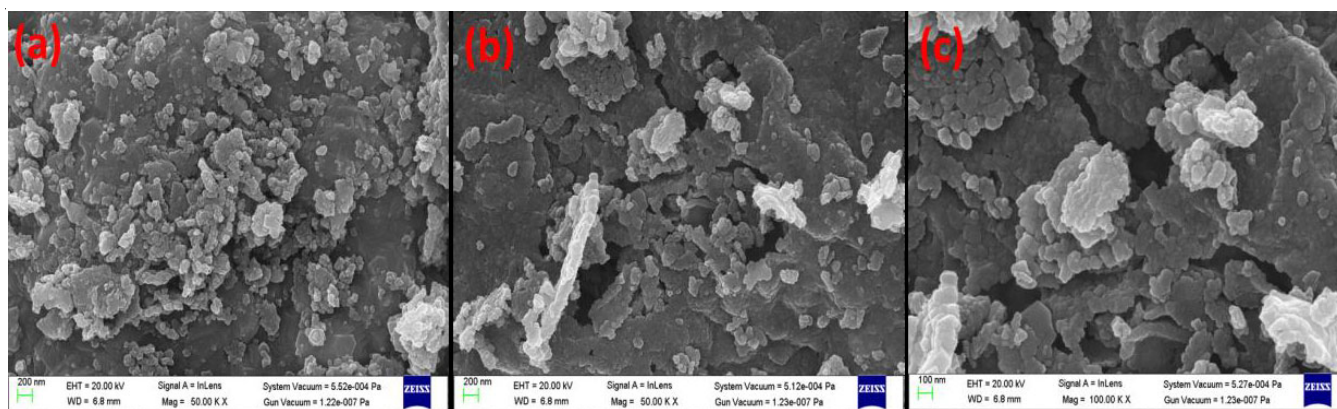
Fig. 3. SEM micrographs of synthesized nanoparticles Cu, $Cu_{0.5}$, $Cu_{0.7}$

Image-J software. In this study, it was observed that the grain size decreases as the dopant concentration increases. The variation in grain size is clearly evident. Based on the FE-SEM images of the investigated nanoferrites, the grain sizes ranged from 16.5 nm to 22 nm, indicating a reduction with increasing dopant concentration. The nanoscale nature of the synthesized nanoferrites was confirmed by these grain size measurements and the doping effects on the base ferrite compound. Fig. 4 confirms the presence of elemental confirmation shown the weight percentage of the same.

UV-absorption spectral studies: The UV-visible absorption (Fig. 5a) exposes interesting information about the optical characteristics of copper and its doped materials. The black line illustrates pure copper with unique absorbance peaks at 200-900 nm wavelengths, suggesting strong electronic transitions. When copper is doped at concentrations of 0.7 (red line) and 0.5 (green line), these peaks move slightly, indicating changes in the electronic structure caused by doping. The differences in peak intensities and placements indicate that doping modifies the optical behaviour of material, potentially increasing its appropriateness for applications in electronics and photonics.

Element	Weight (%)	Atomic (%)
O	25.71	54.43
Mg	3.55	4.94
Fe	47.28	28.67
Ni	5.44	3.14
Cu	14.41	7.68
Ag	3.61	1.13
Total	100.00	100.00
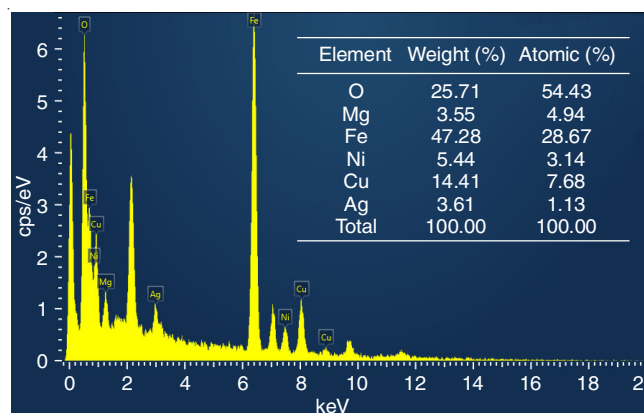
Fig. 4. EDX spectra of synthesized nanoparticles $Cu_{0.7}$

This graph emphasizes the relevance of doping in modifying material characteristics for various technological applications, transforming it into an essential tool for researchers and engineers in the discipline [20-23].

The direct band gap (Fig. 5b) derived from the UV-visible data illustrates the impact of doping on copper's electrical
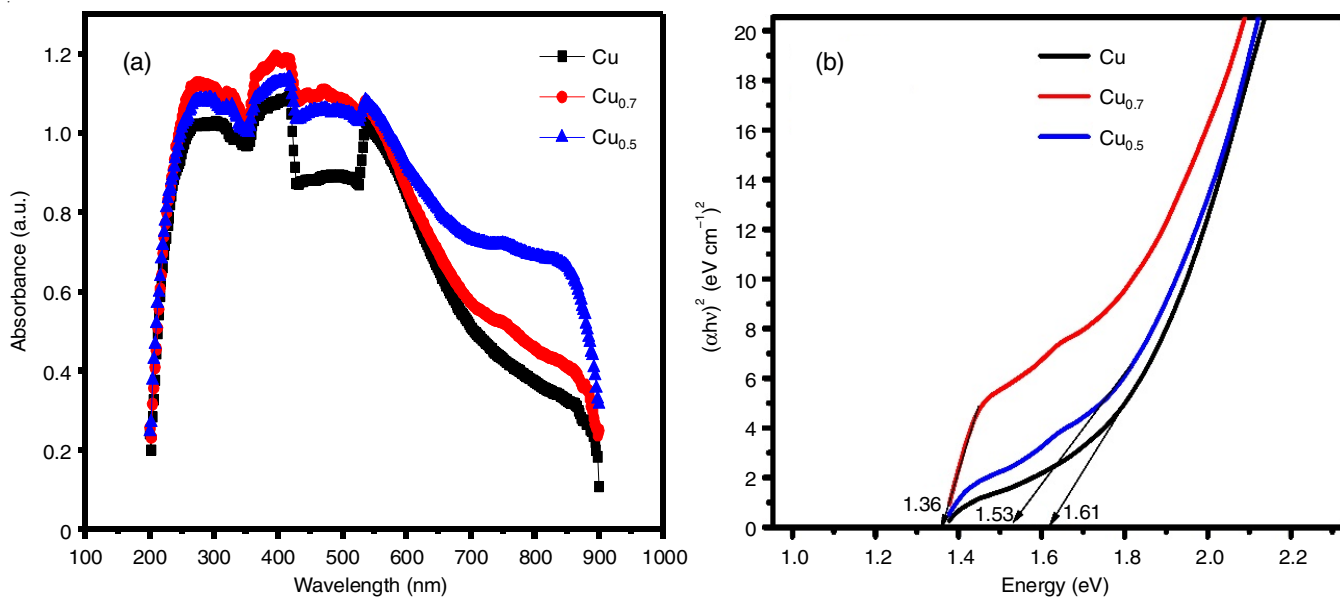
Fig. 5. (a) UV spectra and (b) direct band gap of synthesized nanoparticles Cu, $Cu_{0.5}$, $Cu_{0.7}$
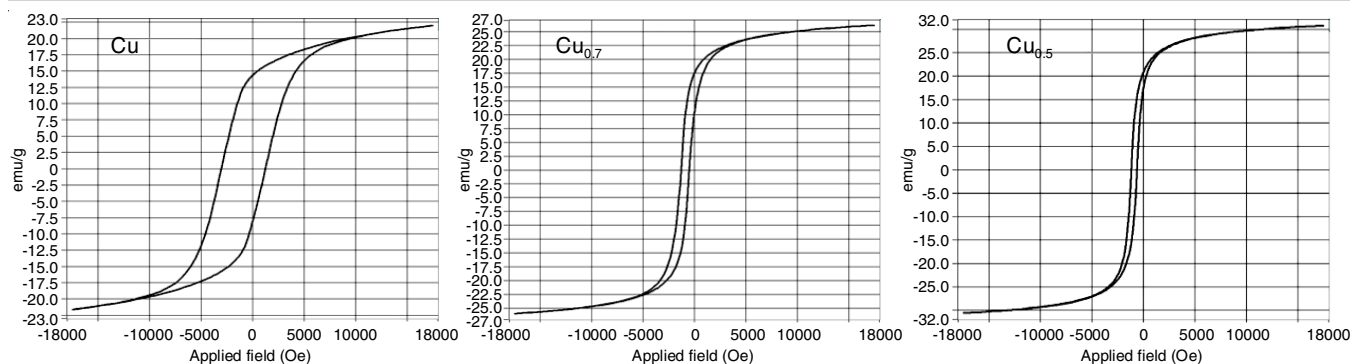
Fig. 6. Magnetic properties of Cu, Cu$_{0.5}$ and Cu$_{0.7}$

properties. The black line represents pure copper, which has a band gap of 1.61 eV, whereas copper doped at 0.7% has a lower direct band gap of 1.36 eV; similarly, copper doped at a concentration of 0.5 has a straight band gap of 1.53 eV. These changes in band gap values demonstrate how doping modifies copper's electrical structure, possibly increasing its appropriateness for a variety of applications in electronics and optoelectronics. By decreasing the band gap, doping enhances the material's optical absorption properties and conductivity, making it more efficient for use in sensors and solar cells [24-26].

Magnetic studies: Magnetic measurements of the prepared nanoferrites were conducted using a vibrating sample magnetometer at room temperature, with an applied field of 20 kOe. The resulting hysteresis loop illustrates the relationship between the magnetization (M) and the applied magnetic field (H). The key magnetic parameters include saturation magnetization (Ms), which is the maximum value of magnetization; remanent magnetization (Mr), the magnetization at zero field; and Coercivity (Hc), the magnetic field required to reduce the magnetization of the material to zero after the sample has been saturated. The chemical composition, porosity and grain size of the ferrite compound significantly influenced the shape and width of the hysteresis loops.

The hysteresis loop of CuFe$_2$O$_4$ nanoparticles was studied to examine their magnetic properties (Fig. 6). For Cu, the remanent magnetization (Mr) is 0.93 emu/g, the coercive field (Hc) is 1252 Oe and the magnetization at saturation (Ms) is estimated to be only 22.30 emu/g, respectively. For Cu$_{0.5}$, the remanent magnetization (Mr) is 1.32 emu/g, the coercive field (Hc) is 509 Oe and the magnetization at saturation (Ms) is estimated to be only 26.02 emu/g, respectively. Finally, for Cu$_{0.7}$, the remanent magnetization (Mr) is 2.14 emu/g, the coercive field (Hc) is 1592 Oe and the magnetization at saturation (Ms) is estimated to be only 29.92 emu/g, respectively [27,28].

Conclusion

The sol-gel technique was employed to synthesize copper-magnesium-nickel doped silver nanoferrites and characterized. Based on the XRD data, the size of the crystallites was observed to range between 20 to 26 nm. FTIR examination revealed metal ion peaks at 547 cm^{-1} to 569 cm^{-1}. FESEM showed non-uniform pattern images. Elemental analysis revealed the presence of copper, magnesium, nickel and silver in the doped nanoferrites. UV-visible spectroscopy revealed a direct optical band gap, 1.61 eV for Cu, 1.36 eV for Cu$_{0.7}$ and 1.53 eV for Cu$_{0.5}$, respectively. The hysteresis loop of CuFe$_2$O$_4$ nanoparticles was studied to examine their magnetic properties. The results indicate that the synthesized nanoferrites may be useful in semiconducting devices and magnetic data storage.

CONFLICT OF INTEREST

The authors declare that there is no conflict of interests regarding the publication of this article.

REFERENCES

1. V.K. Surashe, V. Mahale, A.P. Keche, R.C. Alange, P.S. Aghav and R.G. Dorik, *J. Phys.: Conf. Ser.*, **1644**, 012025 (2020);
https://doi.org/10.1088/1742-6596/1644/1/012025

2. M. Selvakumar, S. Maruthamuthu, G.S. Thirunavukkarasu, A.T. Dhiwahar, M. Seyedmahmoudian, A. Stojcevski and V.R. Minnam Reddy, *J. Nanopart. Res.*, **24**, 205 (2022);
https://doi.org/10.1007/s11051-022-05582-5

3. T.F. Marinca, I. Chicinas and O. Isnard, *Ceram. Int.*, **39**, 4179 (2013);
https://doi.org/10.1016/j.ceramint.2012.10.274

4. P. Thakur, N. Gahlawat, P. Punia, S. Kharbanda, B. Ravelo and A. Thakur, *J. Supercond. Nov. Magn.*, **35**, 2639 (2022);
https://doi.org/10.1007/s10948-022-06334-1

5. B. Jeevanantham, Y. Song, H. Choe and M. Shobana, *Mater. Lett. X*, **12**, 100105 (2021);
https://doi.org/10.1016/j.mlblux.2021.100105

6. T.R. Jeena, M. Geetha, P. Suchetan, N. Ronald and K. Amrutha, *Inorg. Chem. Commun.*, **157**, 111232 (2023);
https://doi.org/10.1016/j.inoche.2023.111232

7. K. Patil, S. Kadam, P. Lokhande, S. Balgude and P. More, *Solid State Commun.*, **337**, 114435 (2021);
https://doi.org/10.1016/j.ssc.2021.114435

8. A. Solunke, V.K. Barote, B.B. Sonawane, S.E. Shirsath, R. Kadam and V.S. Shinde, *Mater. Today Proc.*, **92**, 1225 (2023);
https://doi.org/10.1016/j.matpr.2023.05.327

9. V. Bhagwat, A.V. Humbe, S.D. More and K.M. Jadhav, *Mater. Sci. Eng. B*, **248**, 114388 (2019);
https://doi.org/10.1016/j.mseb.2019.114388

10. M.N. Kiani, M.S. Butt, I.H. Gul, M. Saleem, M. Irfan, A.H. Baluch, M.A. Akram and M.A. Raza, *ACS Omega*, **8**, 3755 (2023);
https://doi.org/10.1021/acsomega.2c05226

11. M.Y. Wani, A.A. Pandit, J. Begum, N. Ahmed, M.S. Mir and D.M. Makhdoomi, *Lett. Anim. Biol.*, **2**, 32 (2022);
https://doi.org/10.62310/liab.v2i1.77

12. D. Mallesh, P. Naresh, G. Thalari and A. Seema, *ECS J. Solid State Sci. Technol.*, **13**, 043004 (2024);
https://doi.org/10.1149/2162-8777/ad3982

13. S.K. Pradhan, S. Bid, M. Gateshki and V. Petkov, *Mater. Chem. Phys.*, **93**, 224 (2005);
https://doi.org/10.1016/j.matchemphys.2005.03.017

14. P. Mitra, N. Jahangeer and B.H. Venkataraman, *ECS J. Solid State Sci. Technol.*, **13**, 033002 (2024);
https://doi.org/10.1149/2162-8777/ad2e1b

15. M. Tanveer, I. Nisa, G. Nabi, M. Khalid Hussain, S. Khalid and M.A. Qadeer, *J. Magn. Magn. Mater.*, **553**, 169245 (2022);
https://doi.org/10.1016/j.jmmm.2022.169245

16. M. Raghasudha, D. Ravinder and P. Veerasomaiah, *J. Magn. Magn. Mater.*, **355**, 210 (2014);
https://doi.org/10.1016/j.jmmm.2013.12.020

17. M. Raghasudha, D. Ravinder and P. Veerasomaiah, *J. Chem.*, **2013**, 804042 (2013);
https://doi.org/10.1155/2013/804042

18. D. Ravi Kumar, C.A. Lincoln, G. Vijaya Charan, G. Thara, D. Ravinder, M. Veeraswamy and P. Naresh, *Mater. Chem. Phys.*, **278**, 125648 (2022);
https://doi.org/10.1016/j.matchemphys.2021.125648

19. M.A. Dar, V. Verma, S.P. Gairola, W.A. Siddiqui, R.K. Singh and R.K. Kotnala, *Appl. Surf. Sci.*, **258**, 5342 (2012);
https://doi.org/10.1016/j.apsusc.2012.01.158

20. D.R. Kumar, S.I. Ahmad, Ch.A. Lincoln and D. Ravinder, *Journal of Asian Ceramic Societies*, **7**, 53 (2019);
https://doi.org/10.1080/21870764.2018.1563036

21. S.B. Somvanshi, S.A. Jadhav, M.V. Khedkar, P.B. Kharat, S.D. More and K.M. Jadhav, *Ceram. Int.*, **46**, 13170 (2020);
https://doi.org/10.1016/j.ceramint.2020.02.091

22. D. Furman, J. Campisi, E. Verdin, P. Carrera-Bastos, C. Franceschi, S. Targ, L. Ferrucci, D.W. Gilroy, A. Fasano, G.W. Miller, A.H. Miller, A. Mantovani, C.M. Weyand, N. Barzilai, J.J. Goronzy, T.A. Rando, R.B. Effros, A. Lucia, N. Kleinstreuer and G.M. Slavich, *Nat. Med.*, **25**, 1822 (2019);
https://doi.org/10.1038/s41591-019-0675-0

23. S. Russo, *Tech. Reg. Anesth. Pain Manage.*, **12**, 105 (2008);
https://doi.org/10.1053/j.trap.2008.01.001

24. R. Srivastava and B.C. Yadav, *Int. J. Green Nanotechnol.*, **4**, 141 (2012);
https://doi.org/10.1080/19430892.2012.676918

25. S. Malvia, S.A. Bagadi, U.S. Dubey and S. Saxena, *Asia Pac. J. Clin. Oncol.*, **13**, 289 (2017);
https://doi.org/10.1111/ajco.12661

26. A. Pourjavadi, S.S. Amin and S.H. Hosseini, *Ind. Eng. Chem. Res.*, **57**, 822 (2018);
https://doi.org/10.1021/acs.iecr.7b04050

27. A. Kannolli, A. P, S.R. Manohara, M. Taj and M.G. Kotresh, *J. Magn. Magn. Mater.*, **584**, 171079 (2023);
https://doi.org/10.1016/j.jmmm.2023.171079

28. A. Kannolli, A. P, A.K. Shettar, J.H. Hoskeri and M.G. Kotresh, *Chem. Phys. Impact*, **7**, 100396 (2023);
https://doi.org/10.1016/j.chphi.2023.100396